ELSEVIER

Journal of Nuclear Materials 290–293 (2001) 1148–1154

journal of nuclear materials

www.elsevier.nl/locate/jnucmat

Section 11. Wall conditioning

Operational limits under different wall conditions on TEXTOR-94

J. Rapp [a,*], W. Biel [a], H. Gerhauser [a], A. Huber [a], H.R. Koslowski [a], M. Lehnen [a], V. Philipps [a], A. Pospieszczyk [a], D. Reiser [a], U. Samm [a], G. Sergienko [b], M.Z. Tokar [a], R. Zagórski [c]

[a] *Institut für Plasmaphysik, Forschungszentrum Jülich GmbH, EURATOM Association, Trilateral Euregio Cluster, D-52425 Jülich, Germany*

[b] *Institute for High Temperatures of RAS, IVTAN Association, Izhorskaya 13/19, Moscow 127412, Russian Federation*

[c] *Institute of Plasma Physics and Laser Microfusion, P.O. Box 49, 00-908 Warsaw, Poland*

Abstract

Generally the operational range of tokamaks is limited by the β and the density limit. Experimentally it was found, that the appearance of MARFEs [B. Lipschultz, J. Nucl. Mater. 145–147 (1987) 15] inhibited an increase of the density significantly above the so-called Greenwald density (n^{GW}) [M. Greenwald et al., Nucl. Fus. 28 (1988) 2199]. In TEXTOR-94 the onset of MARFEs has been investigated under different wall conditions. With fresh siliconization and fresh boronization the appearance of MARFEs can be postponed to higher densities ($N^{GW} = \overline{n}_e/n^{GW} = 1.7$). At those high densities $\overline{n}_e = 8 \times 10^{19}$ m^{-3} the Z_{eff} is reduced to 1.3. But as important as the reduction of the global impurity content is the suppressed carbon release on the high-field-side (HFS) just after wall conditioning. Modeling of the MARFE onset by the codes B2-Eirene and TECXY demonstrates that an instability on the HFS due to deuterium recycling and radiation only leads to the formation of MARFEs at higher line-averaged densities in comparison to calculations which include carbon impurities. Complete suppression of MARFEs has been achieved by controlled displacement of the plasma column to the low-field-side (LFS), which reduces the local recycling and impurity release at the inner bumper limiter. This resulted in the highest densities achieved at TEXTOR-94 of $N^{GW} = 2.1$ independent of wall conditions. In this case the maximum achievable density is limited by a radiative collapse. © 2001 Published by Elsevier Science B.V.

Keywords: Coating; Impurity; Plasma properties

1. Introduction

MHD instabilities and radiation instabilities limit the operational range of tokamaks with respect to maximum pressure and maximum density. The β limit is encountered in high confinement discharges, which are on TEXTOR-94 in the radiative-improved mode (RI-mode) [2]. The β limit under these conditions is caused by the onset of MHD activity in the plasma core and leads to a reduction of the confinement quality down to L-mode level. Because the RI-mode follows the neo-Alcator scaling law, the energy confinement time is proportional to the electron density, it would be advantageous to increase the density above the so-called Greenwald limit. First attempts to achieve this by careful control of the gas fueling have been successful [3]. In the following we will concentrate on the dependence of the density limit on wall conditions in L-mode discharges.

Since the radiation depends strongly on the impurity content of the plasma, the impurity sources, and hence the wall conditions, play an important role in the density limiting process. From the start of operation of TEXTOR the density limit has been increased successfully by

* Tel.: +49-2461 615 102; fax: +49-2461 615 452.
E-mail address: j.rapp@fz-juelich.de (J. Rapp).

0022-3115/01/$ - see front matter © 2001 Published by Elsevier Science B.V.
PII: S0022-3115(00)00553-5

reducing Z_{eff}, which was achieved by wall conditioning methods (i.e. carbonization, boronization) [4]. However, the appearance of the so-called MARFEs, which are poloidally localized radiation zones occurring on the high-field-side (HFS) of the tokamak, inhibited an increase of the density limit significantly above the empirically found Greenwald density. The onset of those MARFEs will be discussed with respect to the scaling with global and edge parameters. Furthermore the influence of the wall conditions on the density limit and in particular the MARFE development is studied. In this respect we limited our investigations to a comparison of boronized and siliconized [5] vessel coatings. Potential differences due to (i) gettering ability of oxygen by the wall coating, (ii) plasma edge properties, (iii) wall pumping capabilities, (iv) impurity release and (v) impurity content are discussed. The experimental findings are compared to analytical models and numerical simulations of MARFEs.

2. Scaling of the MARFE-onset with global and local parameters

Fully developed, the MARFE consists of a cold ($T_e = 1$ eV) and dense ($n_e = 2 \times 10^{20}$ m^{-3}) plasma [6]. The maximum line-averaged density scales linearly with the plasma current [7] and agrees well with the predicted Greenwald limit [1]. If the MARFEs are suppressed [8], by changing the distance of the plasma to the wall surface on the HFS, the Greenwald limit can be exceeded easily by a factor of 2. This phenomenon has been explained by a change in localized recycling on the HFS [9]. In outward shifted plasmas still MARFEs can occur, but the plasma parameters of those MARFEs differ from the one with plasma wall contact ($n_e = 6 \times 10^{19}$ m^{-3}, $T_e = 3$ eV). Those experimental facts put already the validity of the Greenwald limit in question. Since the Greenwald scaling is dependent on the volume-averaged plasma current only, a further test utilizing parameter scans with respect to the global quantities, B_t and P_{heat} have been performed on TEXTOR. A radiative or a thermal instability like an MARFE should appear at higher densities, if only the plasma is heated strong enough. In Fig. 1, $\bar{n}_e^{\text{cr}}$, the electron density just before the MARFE-onset, is shown a function of the total heating power (NBI plus Ohmic heating). Although the heating power is tripled the critical electron density increases only marginally. Since the MARFE is a cooling instability at the plasma edge, the edge plasma parameters rather than line-averaged values should be of importance. In Fig. 2 the critical edge electron densities $n_e^{\text{cr}}(a)$ and the edge electron temperatures are plotted against the heat flux $q_\perp$, which crosses the last closed flux surface (LCFS). It should be mentioned that those values (open symbols) are measured by a helium-beam diagnostic on the low-field-side (LFS) and not on the HFS where the MARFE appears. Additionally, line-averaged values from an interferometer channel on the LFS ($R = 2.225$ m) are shown. Both, critical densities and temperatures, have only a weak dependence on the heat flux in the plasma edge. This is less than observed in other L-mode density limit investigations [10]. The gradients of the density profile in the edge change only moderately, but the decay length of the temperature at the LCFS

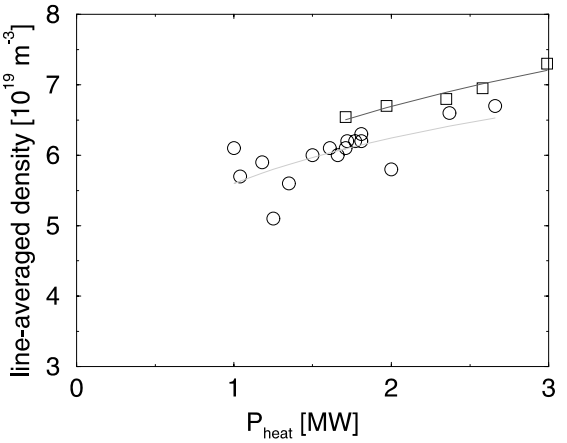

Fig. 1. Critical line-averaged density as function of heating power, carbon dominated (circles), fresh boronization (squares); fit: $P_{\text{heat}}^{0.16}$.

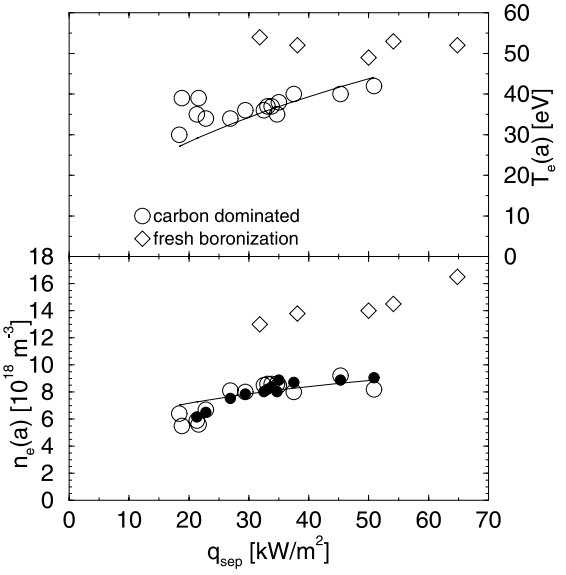

Fig. 2. Critical edge density and critical edge temperature at function of power flux crossing the LCFS, Helium beam data (open symbols), Interferometer data $R = 2.225$ m (a.u.) (filled symbols), carbon dominated (circles), fresh boronization (diamonds); predictions from TECXY (solid lines).

decreases from ≈ 7 cm to almost ≈ 3 cm for the highest heating power.

The determination of the dependence on toroidal magnetic field is limited since it could be varied by a factor of 1.5 only. In Fig. 3 the impact of a B_t variation on the maximum achievable density and the edge parameters is shown. The scaling $\overline{n}_e^{cr} \propto B_t^{-0.5}$ yields a good agreement. On the contrary, $n_e^{cr}(a)$ measured at the plasma edge on the LFS is increasing with increasing magnetic field. The reduction of $\overline{n}_e^{cr}$ with increasing B_t is mainly a plasma profile effect in the plasma boundary, since I_p was held constant and q_a does therefore increase with B_t. This tendency is confirmed with two interferometric line-averaged densities from the plasma boundary (see Fig. 3). Many theories on thermal radiative instabilities imply a critical edge density, which is no function of B_t or even decreasing with increasing B_t. But the increasing $n_e^{cr}(a)$ with magnetic field indicates that the edge density seems to be not responsible for the onset of the MARFE only, specially if one takes into account the fact that the ratio n_e^{HFS}/n_e^{LFS} in the plasma edge is increasing with the toroidal magnetic field, too. A more realistic critical parameter for the MARFE onset seems to be the carbon flux from the bumper limiter on the HFS. This flux is almost independent of variations in the magnetic field and indicates again the important impact of the localized recycling at the HFS on the onset of the MARFE [8,9].

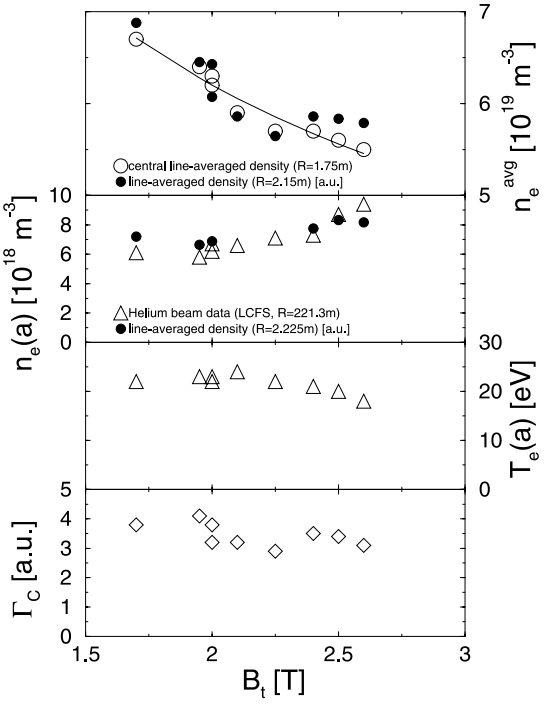

Fig. 3. Critical line-averaged density, edge density, edge temperature, carbon flux at bumper limiter as function of B_t; for comparison: line-averaged densities in the plasma boundary (closed circles).

For this localized recycling instability [9] a criterion for the critical density as function of global plasma parameters can be derived. With the assumption of gyro-Bohm scaling for the diffusion coefficient in the plasma boundary ($D_\perp \propto T_e^{3/2} B_t^{-2} L_n^{-1} \times q_a^2$) [11], $P \propto D_\perp\, T_e n_e / L_n$ and $\kappa_\parallel \propto T_e^{5/2}$ the obtained scaling $\overline{n}_{e,mod}^{cr}$ is very close to the experimental one $\overline{n}_{e,exp}^{cr}$:

$$\overline{n}_{e,exp}^{cr} \propto I_p \times P_{heat}^{0.16} / B_t^{0.5}, \tag{1}$$

$$\overline{n}_{e,mod}^{cr} \propto I_p^{1.14} \times P_{heat}^{0.1} / B_t^{0.48}. \tag{2}$$

In contrast to the findings above, in discharges with plasmas shifted to the LFS the density can be increased until the total radiated power equals the input power and the plasma detaches from the ALT-II limiter [12]. Scalings with respect to global parameters were performed [7] and led to the following critical density for the radiative collapse:

$$\overline{n}_e^{cr} \propto I_p \times P_{heat}^{0.44} / B_t^{0.17}. \tag{3}$$

The dependence on the plasma current is linear as for the MARFE onset, but a significant difference is found in the scaling with the heating power. The edge density shows qualitatively the same dependence as the line-averaged density. Both the dependence on the heating power and the dependence on the toroidal magnetic field can be explained by a simple model, which assumes a poloidally symmetric radiation belt outside the $q = 2$ surface [13].

3. Comparison of fresh siliconization and fresh boronization

With fresh siliconization the appearance of MARFEs can be postponed to higher densities up to $N^{GW} = 1.7$ [14]. The present investigation compares the plasma behavior under freshly siliconized and freshly boronized wall conditions. In Fig. 4 the density limit under fresh siliconized and boronized wall conditions as a function of the averaged plasma current density is shown. For both wall coatings a density limit significantly higher than the Greenwald limit (dashed line) was encountered. Since effects connected with plasma position and aged wall conditions are folded with the effects due to the plasma current variation, a comparison of two discharges with similar boundary conditions (40 discharges after the wall conditioning was applied) is presented in Fig. 5. The comparison shows that the density limit under siliconized wall conditions is higher by about 15%. The differences in the edge density and edge temperature just before the density limit are similarly marginal. For

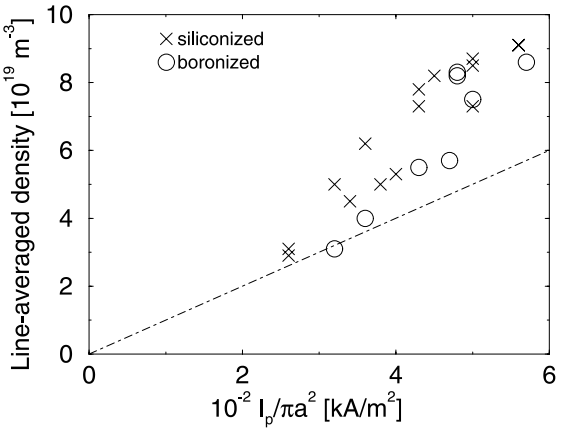

Fig. 4. Density limit for fresh siliconization and fresh boronization, Greenwald limit (dash–dot line); NBI, D→D ($P_{NBI} = 1.35$ MW), $B_t = 2.25$ T.

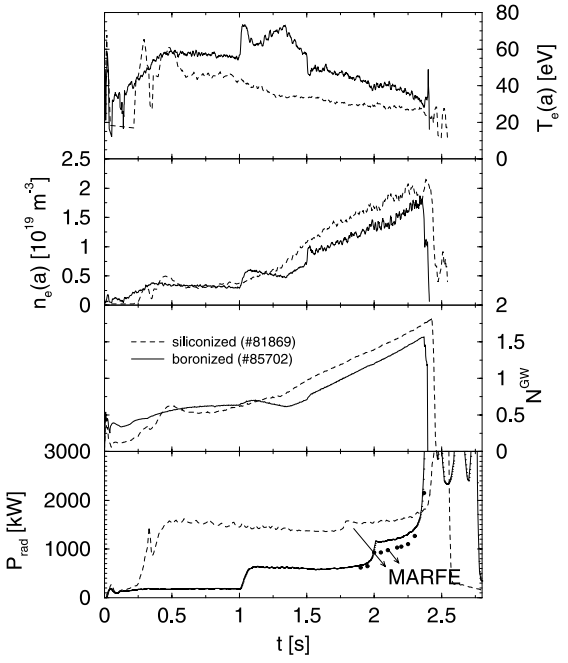

Fig. 5. Comparison of two density limit discharges: fresh boronization (solid line) and fresh siliconization (dashed line), edge temperature, edge density, Greenwald number, total radiated power, total radiated power after tomographic reconstruction (dots); 40 discharges after wall coating procedure, $P_{NBI} = 1.35$ MW (at 0.3 s for siliconization, at 1.0 s for boronization), $I_p = 350$ kA, $B_t = 2.25$ T.

both discharges MARFEs occur at densities of $N^{GW} \approx 1.25$, which are lower than the density limit. The radiated power shown with solid lines in Fig. 5 is derived from a simple integration routine, which does not take into account for strong poloidal asymmetries. For this reason an evaluation of the radiated power from tomographic reconstructions (34 channel bolometry) has been made, which demonstrates that the radiation from the MARFE for boronized and siliconized conditions is quite similarly low (200–250 kW). This is lower by 50% of the radiated power from ordinary MARFEs, occurring in plasmas where carbon was the dominating impurity [7]. Hence the cooling of those MARFEs is not strong enough to hinder the plasma fueling. The fact that the cooling rate of silicon at low electron temperatures does not favor a radiative instability could explain the observed MARFE behavior in principle. Though, the cooling rate of boron is quite similar to that of carbon in the electron temperature range of interest. Thus the difference in radiation characteristic cannot explain the weak MARFEs.

A significant difference between siliconized and boronized wall conditions is observed on the radiated power at low electron densities. This is because of the high plasma contamination at low densities with silicon, which is discussed below.

After fresh boronization also a heating power scan was performed. In general the electron temperatures and electron densities just prior to the density limit are higher after fresh boronization (see Fig. 2). But the scaling with respect to the heating power is quite similar to the heating power scan under aged wall conditions.

3.1. General impurity behavior

In Fig. 6 the Z_{eff} for boronized and siliconized wall conditions demonstrates the strong plasma pollution with silicon at low densities. This is due to physical sputtering, which is strongly reduced at high densities

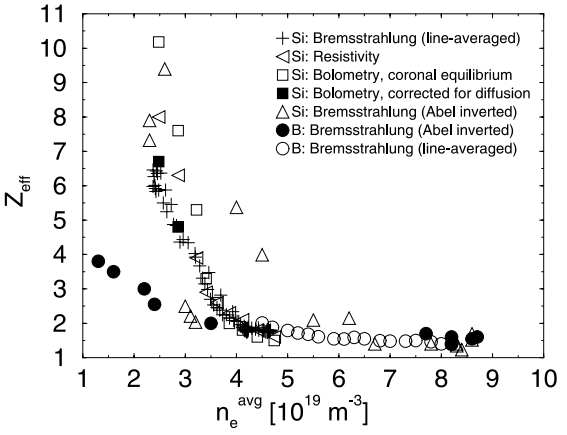

Fig. 6. Z_{eff} as function of line-averaged density, comparison of fresh boronization and fresh siliconization; comparison of different methods: Z_{eff} from bremsstrahlung, resistivity, bolometry (coronal equilibrium and corrected for diffusion $D_\perp = 1$ m^2/s).

and hence low temperatures. Also here the difference between boronization and siliconization at high densities is marginal with the tendency that siliconized wall conditions lead to lower Z_{eff}. The large scatter in Z_{eff} for siliconization at densities $\overline{n}_e = 3\text{–}6 \times 10^{19}$ m^{-3} is due to different discharge series. A comparison of Z_{eff} from bremsstrahlung, resistivity and bolometry gives reasonable agreement. At high densities the Z_{eff} is as low as 1.3.

3.2. Temporal behavior of impurity behavior and discharge quality after wall conditioning

After the wall conditioning the positive effect on the density limit degrades usually shot by shot. This temporal behavior is examined in this chapter.

In Fig. 7 the evolution of spectral line-intensities from several impurity ions is shown for boronization and siliconization. The radiation from both wall coating elements, SiXII (49.94 nm) and BV (4.85 nm), disappears after 40 discharges. In the same time the carbon radiation, CIII (97.7 nm), is increasing. No clear time evolution is seen in the oxygen radiation, OVI (103 nm) and OV (62.9 nm). Together with oxygen, carbon is the dominating impurity 30–40 discharges after wall conditioning again. It seems that the O-radiation is less under siliconized wall conditions, revealing the stronger gettering ability of oxygen (Si: bond energy per oxygen atom is 428 kJ/mol, as compared to B: 397 kJ/mol; furthermore SiO_2 contains more oxygen than B_2O_3). This could explain the lower Z_{eff} for siliconization at high densities (compare Fig. 6), and is in agreement with previous investigations [5].

In Fig. 8, the development of the density limit as a function of the number of shots after boronization is shown. The first 3 discharges in the diagram have been chosen to be comparable in plasma position and heating. After ≈ 300 discharges the density limit is down to $N^{GW} \approx 1$ again. The scatter in those points is due to variations in plasma position and heating. Additionally the carbon fluxes at the main toroidal limiter ALT and the bumper limiter are shown in Fig. 8 for boronization. In agreement with previous observations after siliconization [15] the carbon fluxes from the toroidal ALT saturate already after 30 discharges. At the bumper limiter the carbon fluxes increase less in time, which is demonstrated with two diagnostic set-ups, one viewing line tangential to the bumper limiter and one viewing line perpendicular to the bumper limiter. This is mostly due to a different release mechanism on the bumper limiter. At the bumper limiter chemical erosion is the dominant impurity release mechanism, whereas on the toroidal main limiter ALT-II physical sputtering is more pronounced. But chemical erosion of Boron and Silicon

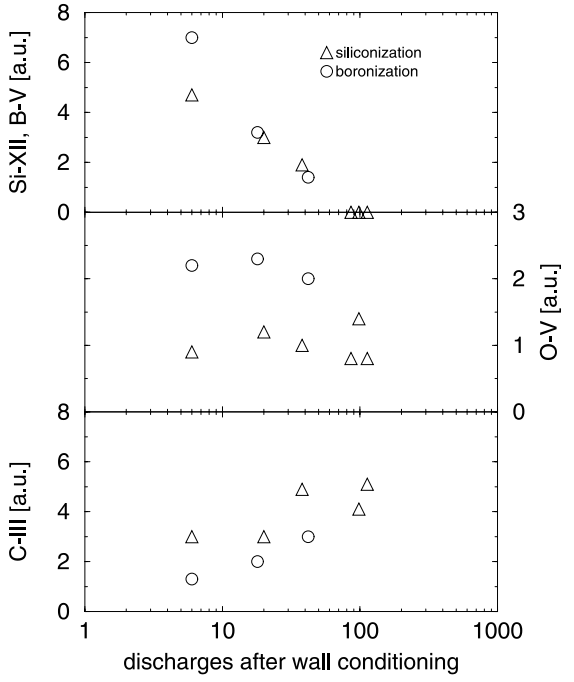

Fig. 7. Temporal evolution of line-intensities of several impurities after wall conditioning, $P_{\text{NBI}} = 1.35$ MW, $\overline{n}_e = 6.8 \times 10^{19}$ m^{-3} for siliconization and $\overline{n}_e = 6.0 \times 10^{19}$ m^{-3} for boronization, $I_p = 350$ kA, $B_t = 2.25$ T.

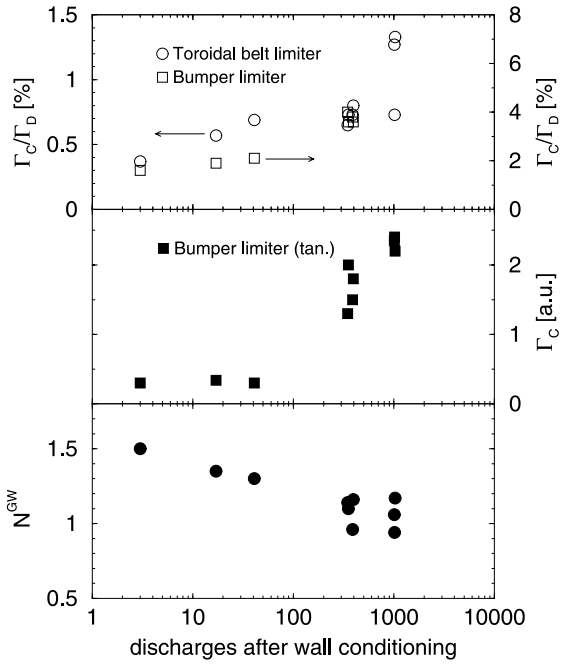

Fig. 8. Temporal evolution of carbon release (Γ_C/Γ_D) from toroidal limiter ALT-II and bumper limiter compared with temporal evolution of density limit after wall conditioning by boronization.

is negligible. The explanation for the observed behavior is, that first the Si- or B-coated surface on highly loaded parts of the ALT-II limiter is eroded and in the following carbon is released on those parts. This leads to an equilibrium after 20–30 discharges in the form of mixed Si/C or B/C layers, respectively. The sputtered carbon from the ALT-II is then distributed in the vessel and leads to a covering of the bumper limiter with carbon.

The increased carbon release from the ALT cannot explain the observed behavior of the MARFE onset, since experiments with shifted plasmas demonstrate that the MARFE onset is postponed to higher densities (+30%) although Γ_C/Γ_D from the ALT increases by a factor of 2.

Also the deuterium flux from the bumper cannot explain the behavior, since it is even slightly decreasing with increasing shot number. The recycling at those high densities does not change significantly in time. It is approximately 96% for all discharges.

Thus the carbon release on the bumper limiter seems to be essential for the development of the MARFE.

4. Modeling

Utilizing feedback control of MARFEs [16] enabled a systematic investigation of spatial radiation distributions from various ionization stages and the total radiated power. Those experimental data could be used for comparison studies with the numerical 2D edge codes TECXY and B2-Eirene [17,18]. Those codes take into account the geometric boundary conditions with respect to the limiters ALT-II and the bumper.

In general the modeling of the MARFE was quite successful with respect to T_e and n_e inside the MARFE. For a comparison the poloidal distributions of the radiated power from carbon derived with B2-Eirene and the tomographic reconstruction of the total radiated power derived from bolometry are shown in Fig. 9(a). Furthermore a comparison of the line-integrated line-intensities from the CIV (580.5 nm) and CIII (229.6 nm) are shown in Fig. 10. Both spatial distributions of MARFE radiation demonstrate the good agreement between the modeling and the experiment.

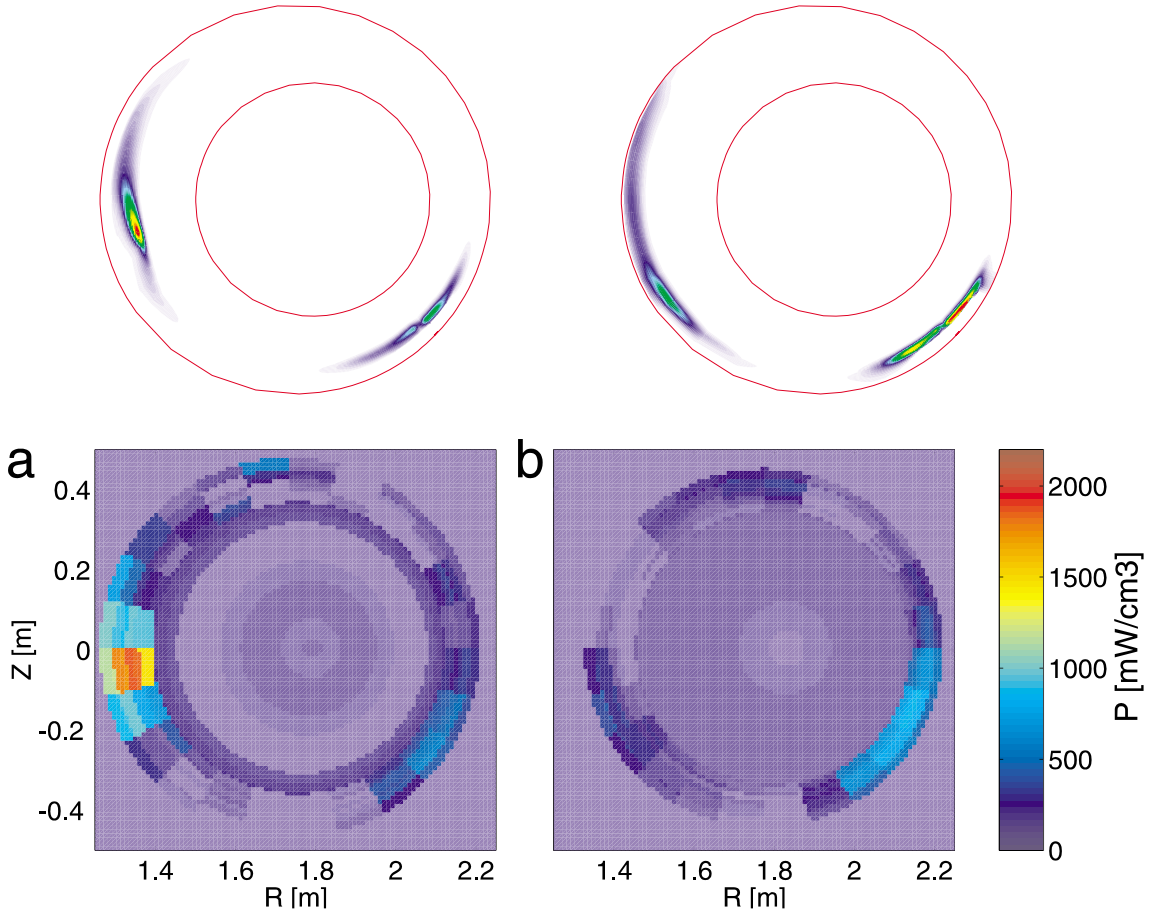

Fig. 9. Comparison of B2-Eirene simulations (total carbon radiation, upper row) with total radiation profiles from bolometry (lower row); distance to bumper in experiment: 1.3 ± 1 cm (a), 4.0 ± 1 cm (b); distance to bumper in simulation: 1.2 cm (a), 3.7 cm (b).

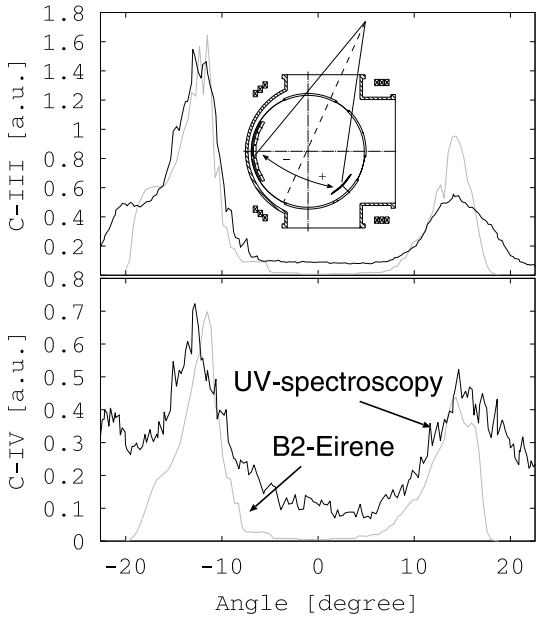

Fig. 10. Comparison of B2-Eirene and experiment: poloidal distribution of C-III and C-IV radiation (line integrals).

In numerical experiments with B2-Eirene the bumper limiter was withdrawn from the plasma, thus increasing the distance from the LCFS to the bumper surface. The radiation from those MARFEs (Fig. 9(b)) is weaker and demonstrates the significance of the plasma wall interaction for the formation of the MARFE.

A variation of the heat flux was performed with TECXY, but without impurities [17]. In Fig. 2 the scaling of the edge density for the MARFE onset is plotted and confirms the weak dependence with the heating power ($n_e^{cr}(a) \propto P_{heat}^{0.23}$). Deviations occur in the scaling of the edge temperature, which is stronger ($T_e^{cr}(a) \propto P_{heat}^{0.48}$) than the dependence obtained experimentally. But in TECXY calculations, which take into account impurities, the critical edge density reduces by $\approx 25\%$. Qualitatively this is in agreement with the observed experimental behavior that the critical edge density is higher after fresh boronization ($n_e^{cr}(a) \approx 1.3 \times 10^{19}$ m^{-3}) and siliconization due to a reduced carbon release on the HFS (see Fig. 2). Again, in comparison with experimental observation, the carbon source from the ALT-II limiter only cannot lead to a MARFE development at those edge densities as modeling with the kinetic code DORIS demonstrated [19].

5. Conclusions

No significant difference between boronization and siliconization with respect to the density limit has been observed. Both, fresh boronization and fresh siliconization allow to increase the density to $\approx 1.7 \times$ the Greenwald density. The reduction of carbon release directly after siliconization and boronization leads to a suppression of MARFEs, which results in a higher density limit. If the plasma wall interaction on the HFS is suppressed completely, by increasing the distance from the LCFS to the HFS, the highest normalized density was reached in TEXTOR. Furthermore, scalings with respect to global and local plasma parameters support the theory of localized recycling as a trigger mechanism for the MARFE onset. Numerical modeling with 2D codes, including the specific geometric boundary conditions of TEXTOR, are in satisfactory agreement with experimental findings and demonstrate the importance of local recycling and impurity release on the HFS for the development of the MARFE.

References

[1] M. Greenwald et al., Nucl. Fus. 28 (1988) 2199.
[2] R.R. Weynants et al., Nucl. Fus. 39 (1999) 1637.
[3] G. Mank et al., Phys. Rev. Lett. 85 (11) (2000) 2312.
[4] J. Winter, J. Nucl. Mater. 176&177 (1990) 14.
[5] U. Samm et al., J. Nucl. Mater. 220–222 (1995) 25.
[6] G. Sergienko et al., in: Proceedings of the 26th International Conference on Plasma Physics Control Fusion, Maastricht, The Netherlands, Europhys. Conf. Abstr., vol. 23J, 1999, p. 725.
[7] J. Rapp et al., Nucl. Fus. 39 (1999) 765.
[8] P.C. de Vries, J. Rapp, F.C. Schüller, M.Z. Tokar, Phys. Rev. Lett. 80 (16) (1998) 3519.
[9] M.Z. Tokar et al., J. Nucl. Mater. 266–269 (1999) 958.
[10] A. Stäbler et al., Nucl. Fus. 32 (1992) 1557.
[11] A. Rogister, Phys. Plasmas 2 (7) (1995) 2729.
[12] J. Rapp et al., in: Proceedings of the 17th IAEA Fusion Energy Conference, Yokohama, Japan, 1998, Fusion Energy (IAEA, Vienna 1999), vol. 2, p. 781.
[13] F.C. Schüller, Plasma Phys. Contr. Fus. 37 (1995) A135.
[14] J. Rapp et al., in: Proceedings of the 26th Conference on Plasma Physics Control Fusion, Maastricht, The Netherlands, Europhys. Conf. Abstr., vol. 23J, 1999, p. 665.
[15] U. Samm, The TEXTOR-94 Team, Plasma Phys. Contr. Fus. 41 (1999) B57.
[16] U. Samm et al., J. Nucl. Mater. 266–269 (1999) 666.
[17] D. Reiser et al., in: Proceedings of the 26th International Conference on Plasma Physics Control Fusion, Maastricht, The Netherlands, 1999, Europhys. Conf. Abstr., vol. 23J, 1999, p. 697.
[18] R. Zagórski et al., Contrib. Plasma Phys. 40 (3 & 4) (2000) 405.
[19] D. Reiser, M.Z. Tokar, in: P. Pavlo (Ed.), Proceedings of the 25th International Conference on Plasma Physics Control Fusion, Prague, Czech Republic, Europhys. Conf. Abstr., vol. 22C (Geneva: European Physical Society), 1998, p. 1828.